Journal of Sound and Vibration 464 (2020) 114982

Contents lists available at ScienceDirect

Journal of Sound and Vibration

journal homepage: www.elsevier.com/locate/jsvi

Methods for evaluating in-duct noise attenuation performance in a muffler design problem

Jong Kyeom Lee, Kee Seung Oh, Jin Woo Lee*

Department of Mechanical Engineering, Ajou University, 206 World Cup-ro, Yeongtong-Gu, Suwon, 16499, Republic of Korea

ARTICLE INFO

Article history:
Received 28 April 2019
Received in revised form 30 August 2019
Accepted 23 September 2019
Available online 26 September 2019
Handling Editor: P. Joseph

Keywords:
Muffler design
Noise attenuation performance
Transmission loss
Insertion loss
Level difference
Topology optimization

ABSTRACT

In this study, methods for evaluating the noise attenuation performance of a muffler in a muffler design problem are investigated, and a proper evaluation method is suggested for actual noise reduction in a duct when an optimally designed muffler is mounted on a duct. Mathematical expressions of the transmission loss, insertion loss, and level difference for a simple expansion chamber muffler are developed from basic acoustic equations. The effects of the locations of the measurement points, tailpipe length, and impedance at the end of the duct on the noise attenuation performance calculated using the three evaluation methods are discussed. The TL and IL maximization problems formulated using topology optimization are solved for a muffler unit, and the noise attenuation performances of the optimally designed mufflers are compared when mounted on a duct. Another acoustical topology optimization problem, a partition volume minimization problem for a muffler design, is formulated to reduce the in-duct broadband noise, and the noise attenuation performance of the optimal muffler obtained using this formulation is experimentally validated. These research results will contribute to the development of a muffler design method with high accuracy by reducing the discrepancy between the noise attenuation performances of a muffler unit and a muffler mounted on a duct.

1. Introduction

Mufflers have been widely used for reducing the flow noise inside a duct, such as in a vehicle exhaust system or the ventilation system of home appliances. In a reactive muffler, internal partitions should be optimally placed to improve the noise attenuation performance in the main noise frequency range when the outer size of the muffler is limited. The high-level noise attenuation performance in the target frequency range was observed in both experiments and numerical analyses of an optimally designed reactive muffler. However, it is often the case that an optimally designed muffler cannot reduce the duct noise when actually mounted on a duct for industrial use. Thus, muffler designers often experience a discrepancy between the noise attenuation performances of a muffler unit and a muffler mounted on a duct. The authors in this paper think that efforts to resolve this discrepancy should focus on methods for evaluating the noise attenuation performance rather than on design methods or the accuracy of the analysis.

* Corresponding author.
E-mail address: jinwoolee@ajou.ac.kr (J.W. Lee).

https://doi.org/10.1016/j.jsv.2019.114982
0022-460X/

Three different evaluation methods were introduced in acoustical analyses and experiments on a muffler unit [1–3]: the transmission loss (TL), insertion loss (IL), and level difference (LD) or noise reduction (NR). Therefore, an exact understanding of each evaluation method, as well as the development of a muffler design method, is required so that the optimally designed muffler should effectively attenuate a target noise when it is mounted on a duct.

The TL is the difference in the sound power level (PWL) of the incident and transmitted waves of a muffler with an anechoic termination [1–3]. Because it is relatively easy to implement an anechoic termination condition at the end of an outlet in theoretical and numerical analyses, the TL has been widely used in muffler design problems based on numerical simulations. Bilawchuk and Fyfe [4] compared several numerical methods to calculate the TL. Åbom [5] derived four-pole parameters including the effects of high-order modes to calculate the TL value of an expansion chamber muffler with an extended inlet and outlet. Selamet and Radavich [6] investigated the effect of the muffler length on its TL. Kirby [7] described a closed-form analytical solution for the TL of a dissipative silencer. Yu and Cheng [8] proposed an analytical approach to calculate the TL of a muffler in the presence of complex internal partitions. However, considerable efforts should be invested in the acoustic experiments for TL measurement to implement the anechoic termination at the end of an outlet and to separate incident and reflected waves in an inlet area [9].

The IL is defined as the difference in the PWL at the same point of an outlet for two cases with and without a muffler [1–3]. Because this method does not require an anechoic termination condition at the end of an outlet, unlike the TL, a single microphone is sufficient to experimentally obtain a frequency-dependent IL curve. Prasad and Crocker [10] obtained the IL curve of a vehicle exhaust system using an acoustical-electric analogy. Craggs [11] used the finite element method to calculate both the IL and TL for reactive mufflers. Ramakrishnan and Stevens [12] improved the accuracy of the IL for a duct silencer. Krüger and Leistner [13] evaluated the noise attenuation performance of actively absorbing silencers by calculating their ILs. Herrin et al. [14] predicted the ILs of large duct systems above the cutoff frequency. In simulation-based muffler analysis and design, however, the accuracy of the calculated IL values strongly depends on the actual radiation impedance imposed at the end of the muffler outlet.

The LD, which is often called the NR (noise reduction), is defined as the difference in the sound pressure level (SPL) between the inlet and outlet of a muffler [1–3]. It is easy to experimentally implement this type of evaluation method and to intuitively understand the SPL reduction achieved through the use of a muffler. Rao and Munjal [15] predicted the LD of an expansion chamber muffler with an offset inlet and outlet and experimentally verified their prediction. However, it is difficult to objectively select the locations of measurement points in the inlet and outlet regions in simulations and experiments [1]. In addition, calculating the LD theoretically or numerically requires the accurate radiation impedance at the outlet end, similar to the IL.

To improve the accuracy of the IL and LD values of a muffler in a simulation, several studies have been conducted to obtain a mathematical expression for the radiation impedance at the ends of outlets with various shapes. Levine and Schwinger [16] developed a simple form of radiation impedance for an unflanged circular pipe, and Norris and Sheng [17] suggested a formula for the radiation impedance of an infinitely flanged circular pipe. Silva et al. [18] presented an approximate mathematical expression of the radiation impedance for a complicated end shape, and Polack et al. [19] presented the relationship between the reflection coefficient and radiation impedance for a circular pipe. Dalmont et al. [20,21] summarized the measurement methods for the radiation impedance and calculated the radiation impedances for several boundary conditions.

In most muffler design problems for noise reduction in a duct, a muffler unit separated from a duct has been used as an analysis model, and TL has been widely used as a method for evaluating the noise attenuation performance of a muffler during the optimization process [22–33]. However, when an optimal muffler obtained through such a design problem is mounted on a duct, its noise attenuation performance may be degraded owing to the moderately long tailpipe and radiation impedance of the duct. The tailpipe length of a muffler mounted on a duct is generally longer than the outlet length of a muffler unit. The actual boundary condition of the tailpipe end is completely different from the ideal boundary condition, namely, the anechoic termination, which is imposed at the end of a muffler for the TL calculation. These facts motivated the authors to compare methods for evaluating the in-duct noise attenuation performance in a muffler design problem and to investigate the effects of the tailpipe length and impedance at the duct end on the optimal design of a muffler mounted on a duct.

This paper compares three well-known methods used to evaluate the noise attenuation performance of a muffler and suggests a proper method among them for an optimal muffler design problem. The criterion is whether an optimally designed muffler can sufficiently attenuate noise in the tailpipe when mounted on a duct. First, mathematical expressions of the TL, IL, and LD are developed from basic acoustic equations, and their particular characteristics are compared. Then, two muffler design problems based on topology optimization are formulated to maximize the TL and IL and are solved for the same design conditions. When optimal mufflers obtained using the TL and IL as methods for evaluating the noise attenuation performance, respectively, are mounted on a duct, the noise levels at the tailpipe of the duct are compared. Finally, with a proper method for evaluating the in-duct noise attenuation performance, another muffler design problem based on topology optimization is formulated to minimize the partition volume and to reduce noise at the target position in a duct. In the theoretical analysis and numerical design, well-known theoretical approaches and acoustical topology optimization problems are recalled. The theoretical and numerical results are discussed to select a proper method for evaluating the in-duct noise attenuation performance in a muffler design problem. The validity of the optimal muffler obtained by solving the formulated problem is experimentally supported.

2. Three methods for evaluating noise attenuation performance

Mathematical expressions of the three methods used to evaluate the noise attenuation performance of a muffler are developed for two ducts with and without an expansion chamber, as shown in Fig. 1(a) and (b). The cross-sectional areas of a duct and an expansion chamber with a length of l are denoted by S_1 and S_2, respectively. The radiation impedance at the end of the ducts is denoted by Z_d. In Fig. 1(b), the duct sections in front of and behind the expansion chamber are called the inlet and the outlet having a length of d, respectively. In general, a muffler unit for analysis and design consists of an inlet, an expansion chamber, and an outlet. One point (P_I), as shown in Fig. 1(a), is selected as the target position, where the SPL is calculated to evaluate the noise attenuation performance of a muffler unit. Two additional points (P_{II} and P_{III}), as shown in Fig. 1(b), are selected for the LD calculation. Points P_I and P_{III} are the same distance away from the ends of the two ducts. It is assumed that only plane waves propagate in the inlet, expansion chamber, and outlet in a low-frequency range without a loss of generality. The plane wave assumption for a theoretical analysis is valid below the cutoff frequency of the expansion chamber, and the specific values will be mentioned in each analysis result.

2.1. Basic equations

The acoustic pressure $p_0(x)$ and particle velocity $u_0(x)$ inside the duct in Fig. 1(a) are expressed as Eq. (1):

$$p_0(x) = A_0 e^{-jkx} + B_0 e^{jkx}, k = \frac{2\pi f}{c}, j = \sqrt{-1}, \tag{1a}$$

$$u_0(x) = \frac{1}{\rho c}\left(A_0 e^{-jkx} - B_0 e^{jkx}\right), \tag{1b}$$

where k is the wave number, and f is the frequency. The density and speed of sound of an acoustic medium are denoted by ρ and c, respectively. The symbols of A_0 and B_0 denote the amplitudes of the forward and backward traveling acoustic waves in a duct, respectively. The reflection coefficient $R_{w/o}$ at the end of a duct without an expansion chamber is expressed as Eq. (2a), and the radiation impedance (Z_d) at the end of the duct is a function of $R_{w/o}$, as in Eq. (2b) [34].

$$R_{w/o} = \frac{B_0 \cdot e^{jk(l+d)}}{A_0 \cdot e^{-jk(l+d)}}, \tag{2a}$$

$$Z_d = Z_0 \cdot S_1 \frac{1 + R_{w/o}}{1 - R_{w/o}}, \tag{2b}$$

where Z_0 indicates the specific acoustic impedance of a duct: $Z_0 = \rho c$.

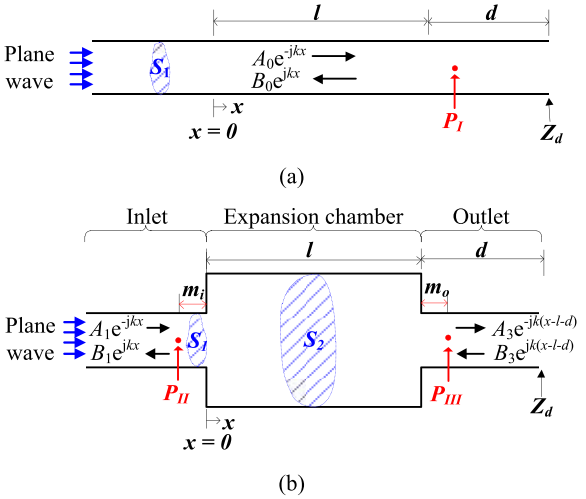

Fig. 1. Analysis models used to develop mathematical expressions for methods used to evaluate noise attenuation performance for a muffler: (a) duct without expansion chamber muffler, and (b) duct with expansion chamber muffler. In both models, a plane wave and radiation impedance (Z_d) are imposed at ends of inlet and outlet, respectively.

The acoustic pressures $p_1(x)$, $p_2(x)$, and $p_3(x)$ in the inlet, expansion chamber, and outlet, as shown in Fig. 1(b), respectively, are expressed as Eq. (3). Particle velocities $u_1(x)$, $u_2(x)$, and $u_3(x)$ are expressed as Eq. (4).

$$p_1(x) = A_1 e^{-jkx} + B_1 e^{jkx}, \tag{3a}$$

$$p_2(x) = A_2 e^{-jkx} + B_2 e^{jkx}, \tag{3b}$$

$$p_3(x) = A_3 e^{-jk(x-l-d)} + B_3 e^{jk(x-l-d)}, \tag{3c}$$

$$u_1(x) = \frac{1}{\rho c}\left(A_1 e^{-jkx} - B_1 e^{jkx}\right), \tag{4a}$$

$$u_2(x) = \frac{1}{\rho c}\left(A_2 e^{-jkx} - B_2 e^{jkx}\right), \tag{4b}$$

$$u_3\left(x\right) = \frac{1}{\rho c}\left(A_3 e^{-jk(x-l-d)} - B_3 e^{jk(x-l-d)}\right), \tag{4c}$$

where A_1, A_2, and A_3 denote the amplitudes of the forward traveling acoustic waves in the inlet, expansion chamber, and outlet, respectively; and B_1, B_2, and B_3 denote the amplitudes of the backward traveling acoustic waves.

At the interfaces ($x = 0$ and $x = l$) between the inlet and the expansion chamber and between the expansion chamber and the outlet, the continuity conditions of the acoustic pressure and volume velocity are expressed as Eq. (5).

$$A_1 + B_1 = A_2 + B_2, \quad S_1(A_1 - B_1) = S_2(A_2 - B_2) \quad at\ x = 0, \tag{5a}$$

$$A_2 e^{-jkl} + B_2 e^{jkl} = A_3 e^{jkd} + B_3 e^{-jkd}, \quad S_2\left(A_2 e^{-jkl} - B_2 e^{jkl}\right) = S_1\left(A_3 e^{jkd} - B_3 e^{-jkd}\right) \quad at\ x = l. \tag{5b}$$

From Eqs. (5a) and (5b), the relationship between $(A_1,\ B_1)$ and $(A_3,\ B_3)$ is obtained in a matrix form in Eq. (6). The matrix component α_i is a function of geometric information $l,\ d,\ S_1,\ S_2$ and wave number k, and the superscript $(^*)$ indicates complex conjugate values. The reflection coefficient R_w at the end of the outlet in Fig. 1(b) is expressed in Eq. (7a), and the radiation impedance Z_d at the outlet is a function of R_w as expressed in Eq. (7b) [34].

$$\begin{Bmatrix} A_1 \\ B_1 \end{Bmatrix} = \begin{bmatrix} \alpha_1 & \alpha_2 \\ \alpha_2^* & \alpha_1^* \end{bmatrix} \begin{Bmatrix} A_3 \\ B_3 \end{Bmatrix}, \tag{6a}$$

$$\alpha_1 = \left(\cos(kl) + j\frac{1}{2}\left(\frac{S_1}{S_2} + \frac{S_2}{S_1}\right)\sin(kl)\right) \cdot e^{jkd}, \tag{6b}$$

$$\alpha_2 = -j\frac{1}{2}\left(\frac{S_1}{S_2} - \frac{S_2}{S_1}\right)\sin(kl) \cdot e^{-jkd}, \tag{6c}$$

$$R_w = \frac{B_3}{A_3}, \tag{7a}$$

$$Z_d = Z_0 \cdot S_1 \frac{1 + R_w}{1 - R_w}\sqrt{a^2 + b^2}. \tag{7b}$$

2.2. Transmission loss

The TL of the expansion chamber muffler in Fig. 1(b) is mathematically expressed as the sound intensity ratio of incident and transmitted waves in Eq. (8) for the same cross section of an inlet and outlet. Using the plane wave theory, the sound intensities of the incident and transmitted waves (I_i and I_t, respectively) are expressed as Eq. (9). When substituting Eqs. (9a) and (9b) for I_i and I_t in Eq. (8), the TL is expressed as a function of the amplitude ratio of the incident and transmitted waves.

$$\mathrm{TL} = 10\log_{10}\left(\frac{I_i}{I_t}\right), \tag{8}$$

$$I_i = \frac{1}{2}\frac{A_1 A_1^*}{\rho c} = \frac{1}{2}\frac{|A_1|^2}{\rho c}, \tag{9a}$$

$$I_t = \frac{1}{2}\frac{A_3 A_3^*}{\rho c} = \frac{1}{2}\frac{|A_3|^2}{\rho c}, \tag{9b}$$

$$\mathrm{TL} = 10\log_{10}\left|\frac{A_1}{A_3}\right|^2. \tag{10}$$

If the anechoic termination condition required for the TL definition is imposed on the end of the outlet ($Z_d = Z_0 \cdot S_1$), then the backward traveling wave in the outlet disappears, namely, $B_3 = 0$ in Eqs. (3c) and (4c). Using Eq. (6a), the TL is expressed as a function of α_1 in Eq. (11a) and becomes the well-known formula in Eq. (11b) when substituting Eq. (6b) for α_1, as in Eq. (11a). The TL in Eq. (11b) is a function of the length of the expansion chamber l, frequency f, and cross-sectional area ratio S_2/S_1 of the expansion chamber and the duct. However, the TL is independent of the outlet length d and the calculation locations of the incident and transmitted acoustic waves.

$$\mathrm{TL} = 10\log_{10}|\alpha_1|^2, \tag{11a}$$

$$\mathrm{TL} = 10\log_{10}\left(\cos^2(kl) + \left(\frac{1}{2}\left(\frac{S_1}{S_2} + \frac{S_2}{S_1}\right)\right)^2 \cdot \sin^2(kl)\right). \tag{11b}$$

2.3. Insertion loss

The duct model in Fig. 1(a) and the muffler model in Fig. 1(b) are required to calculate the IL of a muffler. For the same cross section of an inlet and an outlet, the difference in the PWL at the same point (P_I and P_{III}) for two cases with and without a muffler is replaced by the difference in the sound intensity level expressed in Eq. (12). In this work, an anechoic termination is assumed at the inlet end to neglect the influence of the source impedance on the IL value. That is, a backward traveling acoustic wave in an inlet is not reflected at the inlet end. The sound intensity $I_{\mathrm{w/o}}$ at point P_I and the sound intensity I_w at point P_{III} are calculated using Eqs. (13a) and (13b), respectively. These equations are derived in detail in Appendix A. Considering $R_{\mathrm{w/o}} = R_w$ in Eqs. (2b) and (7b) for the same radiation impedance Z_d at the duct end and the same incident acoustic wave $A_0 = A_1$, the IL is expressed as a function of the amplitude ratio of the incident and transmitted waves in Fig. 1(b), as expressed in Eq. (14). When substituting the amplitude ratio, which is obtained from Eqs. (2a), (6a) and (7a), for A_1/A_3 in Eq. (14), the IL is expressed as a function of α_1 and α_2 with $R(= R_{\mathrm{w/o}} = R_w)$ in Eq. (15a). When substituting Eqs. (6b) and (6c) for α_1 and α_2 in Eq. (15a), the IL is expressed as a function of S_2/S_1, l, f, d, and R, as indicated in Eq. (15b).

$$\mathrm{IL} = 10\log_{10}\frac{I_{\mathrm{w/o}}}{I_w}, \tag{12}$$

$$I_{\mathrm{w/o}} = \frac{1}{2\rho c}\left(A_0 A_0^*\left(1 - R_{\mathrm{w/o}} R_{\mathrm{w/o}}^*\right)\right), \tag{13a}$$

$$I_w = \frac{1}{2\rho c}\left(A_3 A_3^*\left(1 - R_w R_w^*\right)\right), \tag{13b}$$

$$\mathrm{IL} = 10\log_{10}\left|\frac{A_1}{A_3}\right|^2, \tag{14}$$

$$\mathrm{IL} = 10\log_{10}|\alpha_1 + \alpha_2 R|^2, \tag{15a}$$

$$\mathrm{IL} = 20\log_{10}\left|\left(\cos(kl) + \mathrm{j}\frac{1}{2}\left(\left(\frac{S_2}{S_1} + \frac{S_1}{S_2}\right) + R\left(\frac{S_2}{S_1} - \frac{S_1}{S_2}\right)\mathrm{e}^{-\mathrm{j}2kd}\right)\sin(kl)\right)\right|. \tag{15b}$$

Fig. 2(a) compares the IL curves calculated using the IL formula in Eq. (15b) and a commercial finite element analysis program (COMSOL Multiphysics 4.4). The acoustic pressures at points P_I and P_{III} were used in calculating the IL value at each frequency. The cross sections of the expansion chamber and the inlet and outlet were assumed to be a square, and the geometric information used for the calculation is summarized in Table 1. The acoustic medium used in this paper is air unless otherwise

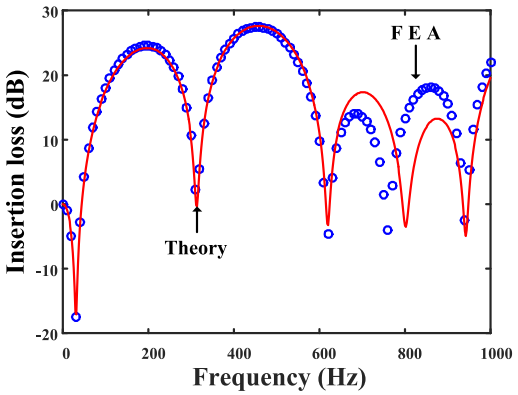

(a)

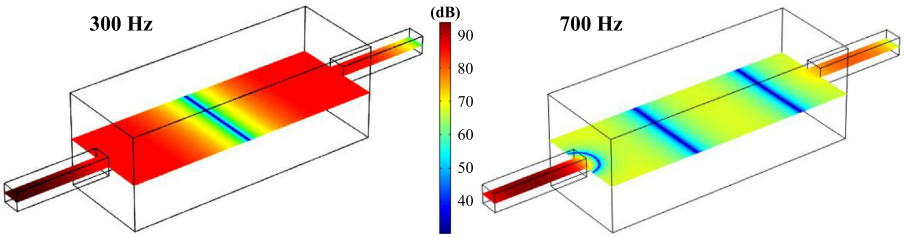

(b)

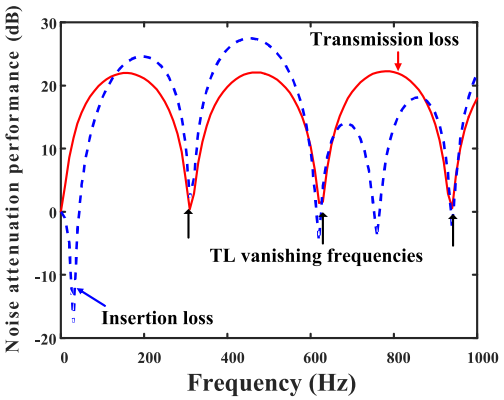

(c)

Fig. 2. Investigation of IL curve: (a) comparison of theoretical and simulated IL curves, (b) comparison of acoustic pressure distributions at 300 and 700 Hz (reference standard pressure: 20×10^{-6} Pa), and (c) comparison of TL and IL curves.

Table 1
Specific values of model parameters used for acoustical analysis.

Symbol	Description	Value (unit)
a_1	One side of cross section of inlet/outlet	0.04 (m)
a_2	One side of cross section of expansion chamber	0.2 (m)
d	Outlet length	0.2 (m)
l	Length of expansion chamber	0.55 (m)

mentioned: $\rho = 1.21$ kg/m^3 and $c = 343$ m/s. The cross-sectional areas S_1 and S_2 of an inlet/outlet and an expansion chamber are denoted by $a_1 \times a_1$ and $a_2 \times a_2$, respectively. The approximate impedance equation in Eq. (16a) suggested by Levine and Schwinger [1,16] was used for the boundary conditions at the ends of the duct and the outlet, and the equivalent radius r in Eq. (16b) was used in calculating R in Eq. (15b) with Eqs. (2b), (7b) and (16a) through a theoretical approach.

$$Z_d = Z_0 \cdot S_1 \left(\frac{k^2 r^2}{4} + \mathrm{j}0.6kr \right), kr < 0.5, \tag{16a}$$

$$r = \sqrt{\frac{a_1^2}{\pi}}. \tag{16b}$$

The theoretical IL curve in Fig. 2(a) agreed well with the simulated IL curve obtained using a finite element analysis for frequencies below 600 Hz. The theoretical IL calculation is not valid above the cutoff frequency (857 Hz) of the expansion chamber. Nevertheless, an obtrusive difference between the two curves started below 857 Hz because of the evanescent wave effect. Evanescent waves with cross modes are generated around an interface owing to the discontinuity in the cross section [35–37]. The effect of the evanescent wave on the acoustical characteristics of the expansion chamber increased with frequency as shown in Fig. 2(b), which displays the acoustic pressure distributions in the middle plane at 300 Hz and 700 Hz. The acoustic pressure distribution around the interface between the inlet and the expansion chamber at 700 Hz is not plane but spherical. Therefore, it was concluded that the derived formula in Eq. (15b) represented well the IL values of the muffler in Fig. 1(b) in a low-frequency range. In addition, the fact that the IL in Eq. (15b) for $R = 0$ is exactly equal to the TL in (11b) supports the validity of the formula in Eq. (15b).

Fig. 2(c) compares the TL and IL curves of the muffler in Fig. 1(b), which were calculated using the specific values provided in Table 1. The two curves started from 0 dB at 0 Hz, but the IL curve decreased with frequency around 0 Hz while the TL increased with frequency around 0 Hz. In addition, while the TL curve had a periodic domelike behavior in a low-frequency range and the TL values were always positive, the IL curve had a nonperiodic domelike behavior and the IL values were positive or negative depending on the frequency region. Moreover, while the TL curve had TL dips at frequencies satisfying the condition of $\sin(kl) = 0$, the IL curve had additional dips at frequencies that were not the TL dip frequencies.

Compared with the TL in Eq. (11b), the IL in Eq. (15b) is a function of the outlet length d and reflection coefficient R as well as the length of the expansion chamber l, frequency f, and cross-sectional area ratio S_2/S_1 of the expansion chamber and duct. This implies that one muffler with the same internal partition layout may have different IL values depending on the radiation impedance and the outlet length. Fig. 3(a) shows the changes in IL depending on the frequency and outlet length d in a two-dimensional color map. The red color indicates a high IL value, and the blue color represents a low IL value. The IL map shows frequency-dependent dips satisfying the condition of $\sin(kl) = 0$, and d (outlet length)-dependent dips, the frequencies of which change with the outlet length d. Fig. 3(b) shows that the IL changes periodically depending on the outlet length at 610 Hz. The distance between two extremely low IL value locations (0.19 m and 0.47 m) approximately coincides with a half-wave length of an acoustic wave at 610 Hz. These results indicate that the in-duct IL of a muffler is strongly affected by the outlet length as well as the frequency.

2.4. Level difference

The level difference (LD) of the muffler in Fig. 1(b) is obtained from the sound pressures measured/calculated at two points (P_{II} and P_{III}) in the inlet and outlet, as expressed in Eq. (17a). The two points are m_i and m_o away from both sides of the expansion chamber, respectively, as shown in Fig. 1(b). The LD is expressed as in Eq. (17b) when using Eqs. (6) and (7), and it shows that the LD depends on the locations of P_{II} and P_{III} as well as the geometric information of the muffler, the reflection coefficient, and the outlet length. This implies that a muffler may have different LD values depending on the location of P_{II} even for a fixed location of P_{III} and the same outlet length.

$$\mathrm{LD} = 20 \log_{10} \left| \frac{p_1(-m_i)}{p_3(l + m_o)} \right|, \tag{17a}$$

$$\mathrm{LD} = 20 \log_{10} \left| \frac{(\alpha_1 + \alpha_2 R) \cdot \mathrm{e}^{\mathrm{j}km_i} + (\alpha_2^* + \alpha_1^* R) \cdot \mathrm{e}^{-\mathrm{j}km_i}}{\mathrm{e}^{-\mathrm{j}k(m_o - d)} + R \cdot \mathrm{e}^{\mathrm{j}k(m_o - d)}} \right|. \tag{17b}$$

Fig. 4(a) compares the LD curves calculated using Eq. (17b) and the commercial finite element analysis program (COMSOL Multiphysics 4.4) for $m_i = 0.1$ m and $m_o = 0.1$ m. The approximate impedance calculated using Eq. (16a) was imposed on the duct end of the same muffler, as in the IL comparison shown in Fig. 3. The theoretical LD curve in Fig. 4(a) agreed well with the simulated LD curve for frequencies below 600 Hz. The difference between the two curves above 600 Hz is also owing to the plane-wave assumption used in the theoretical approach and the evanescent wave effect. Therefore, it can be concluded that Eq. (17b) represents well the LD values of the muffler shown in Fig. 1(b) in a low-frequency range.

Fig. 4(b) shows the LD curve changing with the location of P_{II} for a fixed position of P_{III}: $m_i = 0.02$ m, 0.10 m, and 0.18 m for $m_o = 0.1$ m. The LD curves started from a nonzero dB even at 0 Hz, unlike the TL and IL curves. They decreased with frequency around 0 Hz and had a nonperiodical domelike behavior, as observed in the IL curve. As P_{II} was far away from the entrance of the expansion chamber (as m_i increased), the maximum LD value of the first

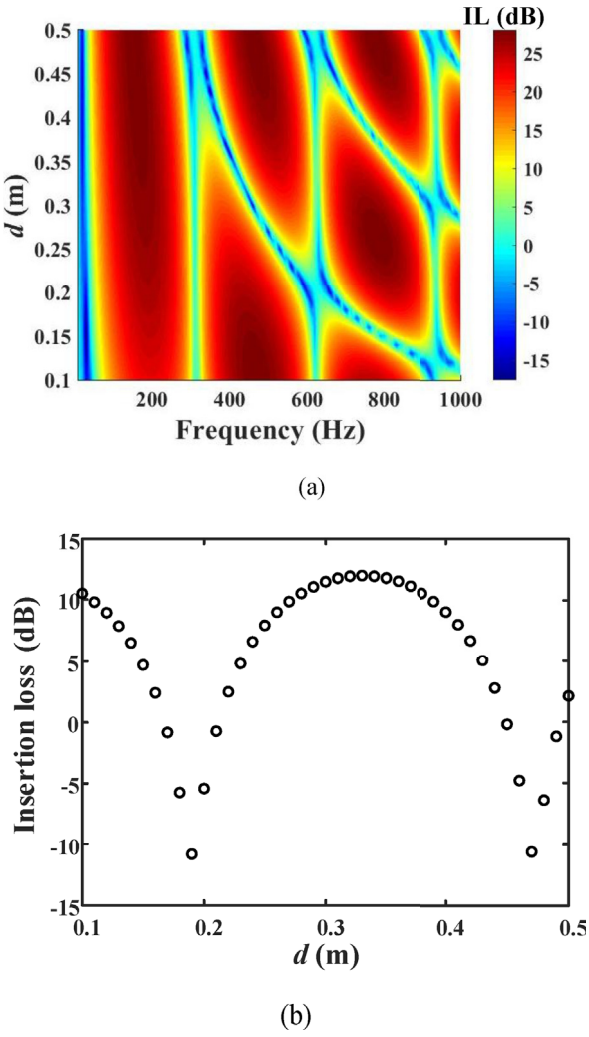

Fig. 3. Investigation of dip frequencies of IL curve: (a) two-dimensional IL map vs. frequency and outlet length, and (b) IL curve changing with outlet length at 610 Hz.

and second domes increased, and the associated frequencies decreased. However, this trend was not seen in the other domes. This phenomenon was also observed when changing P_{III} for a fixed position of P_{II}. These results imply that the LD value changes with the locations (P_{II} and P_{III}) of the measurement points in the inlet and outlet, even for the same muffler. A rational method to objectively select the locations of such points has not been reported yet. Therefore, the LD will not be considered in the following sections that describe optimal muffler design problems.

3. Comparison of TL and IL in muffler design problems based on topology optimization

Many optimal muffler design problems [22–33] have been formulated for a muffler unit separated from a duct, instead of a muffler mounted directly on a duct, and used the TL as a method for evaluating the noise attenuation performance of the muffler used in the design. A muffler unit consists of an expansion chamber, an inlet, and an outlet that is shorter than the tailpipe of the duct. This section investigates the effects of the evaluation method selected in muffler design problems on the actual noise attenuation performance of an optimally designed muffler when mounted on a duct. To this end, two acoustical topology optimization problems are formulated for a muffler design, namely, TL and IL maximization problems. The design goal of the two acoustical topology optimization problems is to decrease the SPL of the expected noise at the target position in a duct. The SPL curve in Fig. 5(a) was numerically calculated at the target position P_{IV} in a duct with a simple expansion chamber muffler that had no internal partition, as shown in Fig. 5(b). In the calculation, the plane wave of the unit magnitude and the radiation impedance in Eq. (16) were imposed on the inlet and outlet ends, respectively. It is assumed that the widths (z-direction) of the muffler and the duct are equal and small compared with their heights and lengths, and they can thus be

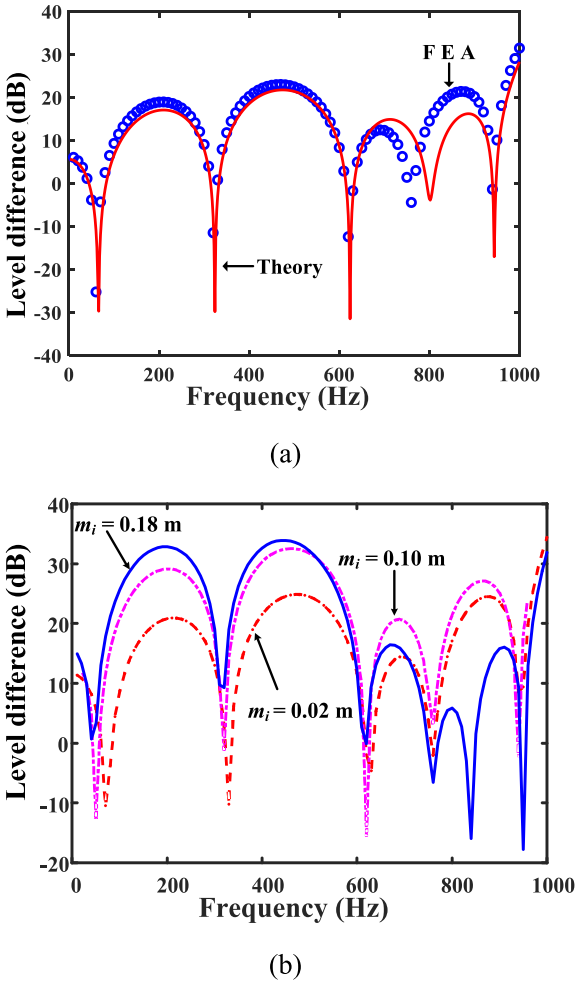

Fig. 4. Investigation of LD curve: (a) comparison of theoretical and simulated LD curves, and (b) effect of location of inlet measurement point (m_i) on LD curve.

regarded as two-dimensional acoustic systems in an acoustical analysis. The specific values of the other parameters necessary for an SPL calculation are summarized in Table 2, and the reference standard pressure is 20×10^{-6} Pa. The optimal muffler obtained in each muffler design problem will be evaluated in terms of how much noise characterized by the SPL curve in Fig. 5(a) will be reduced at P_{IV}.

The finite element models in Fig. 5(c) and (d) are employed for the TL and IL calculations through an acoustical analysis, respectively, and the specific values of the muffler models for a finite element analysis are summarized in Table 2. From Eqs. (10) and (14), TL and IL can be denoted by Γ, which is calculated using Eq. (18) to facilitate the sensitivity analysis indispensable to a gradient-based optimizer. The equation is based on a four-microphone method [38] and is described in detail in Appendix B:

$$\Gamma = 10 \log_{10} \left| \frac{\left(p_a e^{jks_1} - p_b\right)}{\left(p_c e^{jks_2} - p_d\right)} \frac{e^{jks_2} - e^{-jks_2}}{e^{jks_1} - e^{-jks_1}} \right|^2, \tag{18}$$

where p_a and p_b are acoustic pressures at two points s_1 apart from each other in an inlet, and p_c and p_d are acoustic pressures at two points s_2 apart from each other in an outlet, as shown in Fig. 5(c) and (d). For $s_1 = s_2 = s$, acoustic pressures at four points are calculated from the nodal vector of the acoustic pressure ($\mathbf{p}$) obtained through a finite element analysis, as expressed in Eq. (19), where $\mathbf{L}_i$ is the column vector of the unit magnitude at measurement location i ($i = a,b,c,d$) and has the same size as $\mathbf{p}$. Using Eq. (19), Eq. (18) can be converted into Eq. (20).

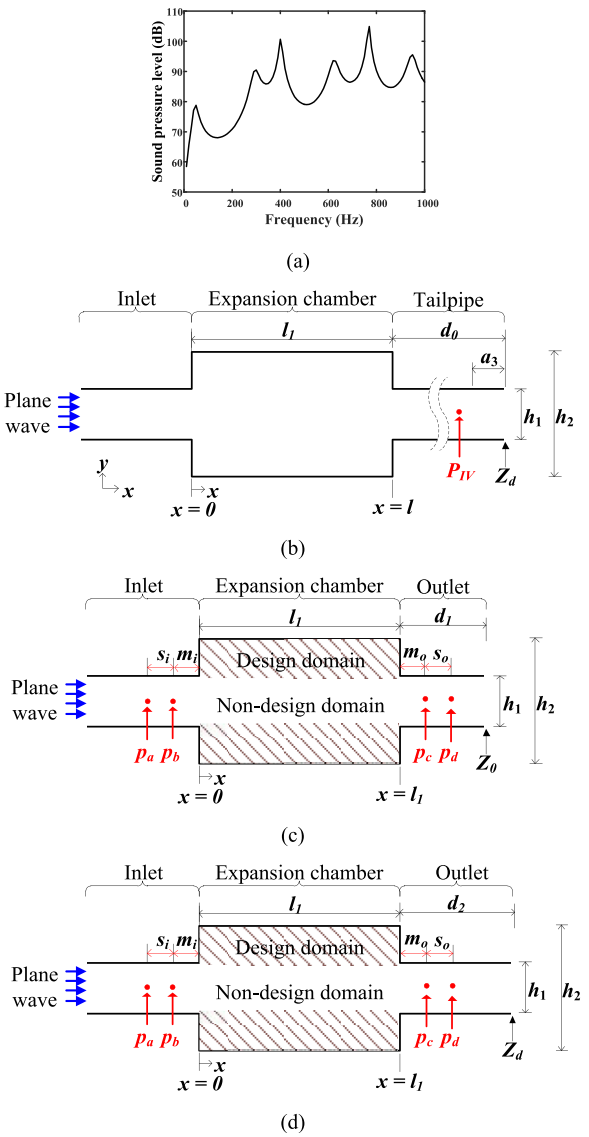

Fig. 5. Acoustic characteristics of nominal muffler and basis models for muffler design problems: (a) SPL curve at target position in duct with simple expansion chamber muffler (reference standard pressure: 20×10^{-6} Pa), (b) muffler mounted on duct, (c) analysis model for TL calculation, and (d) analysis model for IL calculation.

$$p_a = \mathbf{L}_a^T\mathbf{p}, p_b = \mathbf{L}_b^T\mathbf{p}, p_c = \mathbf{L}_c^T\mathbf{p}, p_d = \mathbf{L}_d^T\mathbf{p}, \tag{19}$$

$$\Gamma = 10\log_{10}\left|\frac{\mathbf{q}_1^T\cdot\mathbf{p}}{\mathbf{q}_2^T\cdot\mathbf{p}}\right|^2, \mathbf{q}_1 = \mathbf{L}_a e^{\mathrm{j}ks} - \mathbf{L}_b, \mathbf{q}_2 = \mathbf{L}_c e^{\mathrm{j}ks} - \mathbf{L}_d. \tag{20}$$

For a sensitivity analysis, the following equation was developed [39]:

$$\frac{\partial\Gamma}{\partial\chi_r} = \frac{10}{\ln 10}\times\left(\frac{\mathrm{conj}(\mathbf{q}_1^T\cdot\mathbf{p})\cdot(\mathbf{q}_1^T)}{\mathrm{conj}(\mathbf{q}_1^T\cdot\mathbf{p})\cdot(\mathbf{q}_1^T\cdot\mathbf{p})} - \frac{\mathrm{conj}(\mathbf{q}_2^T\cdot\mathbf{p})\cdot(\mathbf{q}_2^T)}{\mathrm{conj}(\mathbf{q}_2^T\cdot\mathbf{p})\cdot(\mathbf{q}_2^T\cdot\mathbf{p})}\right). \tag{21}$$

where “conj” and “ln” represent a conjugate value and a natural logarithm, respectively.

Table 2
Specific values of model parameters used for acoustical analysis and topology optimization.

Symbol	Description	Value (unit)
a_3	Distance between point P_{IV} and duct end	0.32 m
d_0	Tailpipe length	0.42 m
d_1	Outlet length in Fig. 5(c)	0.2 m
h_1	Height of inlet/outlet duct	0.04 m
h_2	Height of expansion chamber	0.2 m
l_1	Length of expansion chamber	0.55 m
m_1	Distance between p_b and expansion chamber	0.08 m
m_2	Distance between p_c and expansion chamber	0.08 m
s_1	Distance between p_a and p_b	0.02 m
s_2	Distance between p_c and p_d	0.02 m

3.1. Transmission loss maximization problem

A TL maximization problem is formulated for a finite element model, which is divided into a design domain and a non-design domain for the fluid passage, as shown in Fig. 5(c). In general, outlet length d_1 is set to be smaller than tailpipe length d_0, as shown in Fig. 5(b), because the outlet length does not affect the TL value of the muffler, as shown in Eq. (11b): $d_1 < d_0$. The acoustical topology optimization problem formulated by Lee and Kim [26] is recalled for the muffler design:

$$\min \quad \text{obj}, \text{obj} = -\text{TL}_{f=f_t}, \tag{22a}$$

$$\int \chi_r dV \Big/ V \le V_r. \tag{22b}$$

where f_t is the target frequency, and χ_r is the design variable assigned at each node in the design domain. The allowed volume ratio of the rigid partitions and the design domain of volume V is denoted as V_r. The density and bulk modulus ($B = \rho c^2$) of the acoustic finite element are determined by the interpolation functions in Eqs. (23a) and (23b), respectively.

$$\rho_r(\chi_r) = \frac{1}{\frac{1}{\rho_{\text{air}}} + \chi_r\left(\frac{1}{\rho_{\text{air}}} - \frac{1}{\rho_{\text{rigid}}}\right)}, \tag{23a}$$

$$B_r(\chi_r) = \frac{1}{\frac{1}{B_{\text{air}}} + \chi_r\left(\frac{1}{B_{\text{air}}} - \frac{1}{B_{\text{rigid}}}\right)}, \tag{23b}$$

where the subscripts "air" and "rigid" indicate the air and rigid body elements, respectively. The design variable χ_r changes between "0" and "1" during the optimization process and is pushed to one of two limiting values by the interpolation functions. When χ_r becomes "0," the associated finite element is filled with air. By contrast, when χ_r becomes "1," the associated finite element is filled with rigid material. In a successfully converged final topology, all design variables would converge close to "0" or "1." The used interpolation functions in Eq. (23) have already been validated for this type of acoustical topology optimization problem in many previous research results [26–31,39]. The values of ρ_{rigid} and B_{rigid} are determined using Lee and Kim's proposed method [40]: $\rho_{\text{rigid}} = \rho_{\text{air}} \times 10^7$ kg/m^3, $B_{\text{rigid}} = B_{\text{air}} \times 10^9$ Pa, $\rho_{\text{air}} = 1.21$ kg/m^3, and $B_{\text{air}} = 1.42 \times 10^5$ Pa. A plane wave of the unit magnitude and an anechoic termination condition are imposed on the inlet and outlet, respectively, and a rigid wall condition is imposed on the other boundaries.

The TL maximization problem was solved by following the iterative calculation algorithm in Fig. 6(a) for two cases: $f_t = 630$ Hz and $V_r = 0.0445$ in Case A-1, and $f_t = 780$ Hz and $V_r = 0.0662$ in Case A-2. The pressure acoustics module and the optimization module in COMSOL Multiphysics 4.4 was employed with a gradient-based optimizer, namely, the method of moving asymptotes (MMA) [41]. In each case, an acoustical analysis was first conducted using the pressure acoustics module, and then an objective function evaluation and a sensitivity analysis were performed using the optimization module. These results were used for design variable update by employing the MMA. If the updated design variables satisfied the convergence criterion, then the iterative calculation procedure was stopped. Otherwise, the acoustical analysis for the updated design variables was restarted.

The TL value of the simple expansion chamber muffler is almost zero at the first target frequency of 630 Hz, and the SPL curve has a peak value at the second target frequency of 780 Hz, as shown in Fig. 5(a). Fig. 7(a) and (b) show two optimal topologies for Cases A-1 and A-2. In the optimal topologies, the black areas represent rigid partitions. Fig. 7(c) shows the optimization histories of the TL value at the target frequency with several intermediate and optimal topologies during the

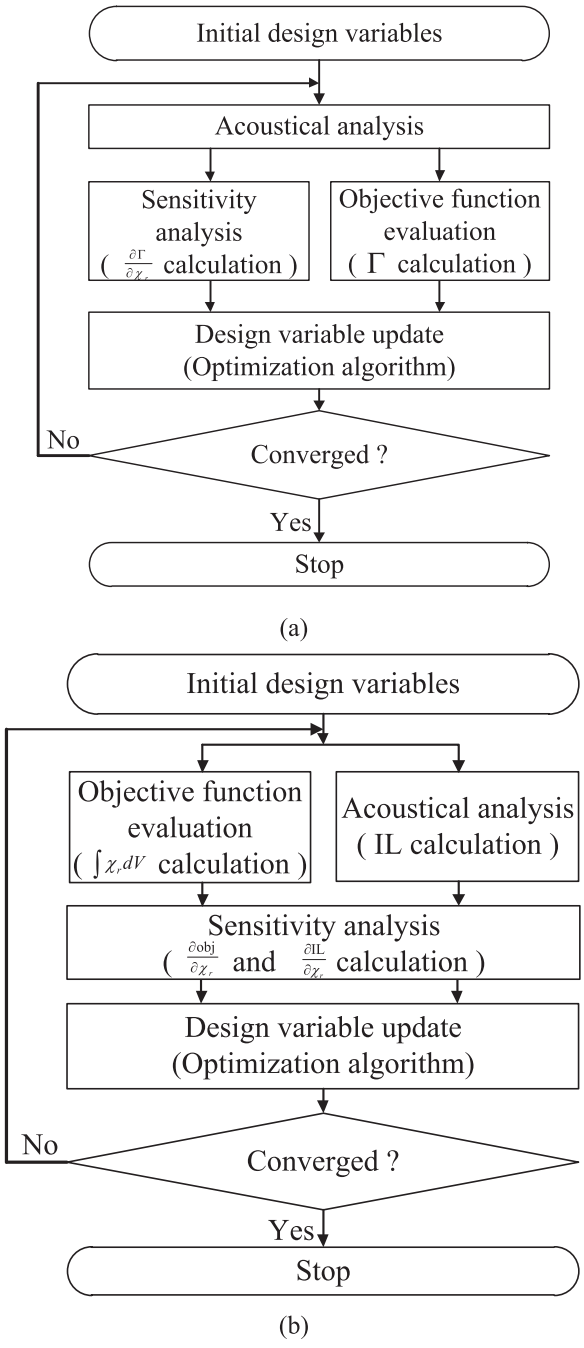

Fig. 6. Flowchart to solve formulated acoustic topology optimizations: (a) TL or Il maximization problem and (b) partition volume minimization problem.

optimization process for both cases. In each case, the optimization process was stopped based on the convergence criterion of $|(\chi_r)_{\text{new}} - (\chi_r)_{\text{old}}| \leq \varepsilon$ for all χ_r, where $(\chi_r)_{\text{new}}$ and $(\chi_r)_{\text{old}}$ denote the current and previous values of the design variables, respectively. The value of ε was set to 10^{-4} in this work after comparing the total computation times and the black and white distributions of final topologies for $\varepsilon = 10^{-2}$, 10^{-2}, 10^{-3}, 10^{-4}, 10^{-5}, and 10^{-6} [42].

In Fig. 8(a), the TL curves of the optimal topologies are compared with that of a simple expansion chamber muffler, which is denoted by a nominal muffler. The TL value at the target frequency was increased by 7.74 dB and 24.42 dB in the two cases, respectively. Fig. 8(b) compares the SPL curves at the target position P_{IV} when the optimal mufflers in Fig. 7(a) and (b) are individually mounted on a duct, as shown in Fig. 5(b). While the SPL at $f_t = 780$ Hz decreased when the optimal muffler in

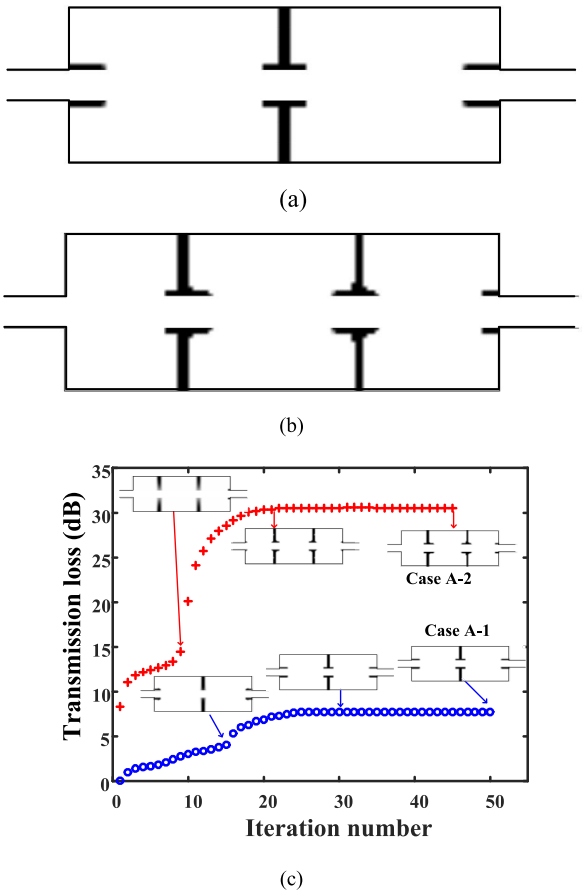

Fig. 7. Design results of TL maximization problem: (a) optimal topology in Case A-1, (b) optimal topology in Case A-2, and (c) optimization history.

Case A-2 was mounted on a duct, the SPL at $f_t = 630$ Hz unexpectedly increased rather than decreased when the optimal muffler in Case A-1 was mounted on a duct. This result demonstrates that an optimal muffler obtained by solving the TL maximization problem cannot always decrease the SPL when mounted on a duct.

3.2. Insertion loss maximization problem

An IL maximization problem based on topology optimization is formulated by replacing the TL in Eq. (22a) with the IL, as expressed in Eq. (24), for the acoustic system shown in Fig. 5(d) and using the same constraint as in Eq. (22b). The outlet length d_2 in Fig. 5(d) is set equal to the tailpipe length d_0 because the outlet length strongly affects the IL value, as shown in Eq. (15b) and Fig. 3(b):

$$\min \ \text{obj}, \text{obj} = -\text{IL}_{f=f_t}, \tag{24a}$$

$$\int \chi_r dV \Big/ V \le V_r. \tag{24b}$$

A plane wave of the unit magnitude and the appropriate impedance in Eq. (16a) are imposed on the inlet and outlet, respectively, and a rigid wall condition is imposed on the remaining boundaries. The same interpolation functions in Eqs. (23a) and (23b) are also used.

The formulated IL maximization problem was solved for the same target frequency and allowed volume ratio as in the TL maximization problem by following the iterative calculation algorithm in Fig. 6(a): $f_t = 630$ Hz and $V_r = 0.0445$ in Case B-1, and $f_t = 780$ Hz and $V_r = 0.0662$ in Case B-2. The obtained optimal topologies are displayed in Fig. 9(a) and (b), and are totally different from those in Fig. 7(a) and (b). For $f_t = 630$ Hz with $V_r = 0.0445$, whereas Case A-1 in Fig. 7(a) had two vertical partitions with horizontal partitions at their ends around the center of the expansion chamber and four horizontal partitions around the inlet and outlet, Case B-1 in Fig. 9(a) had four vertical partitions without horizontal partitions around the inlet and

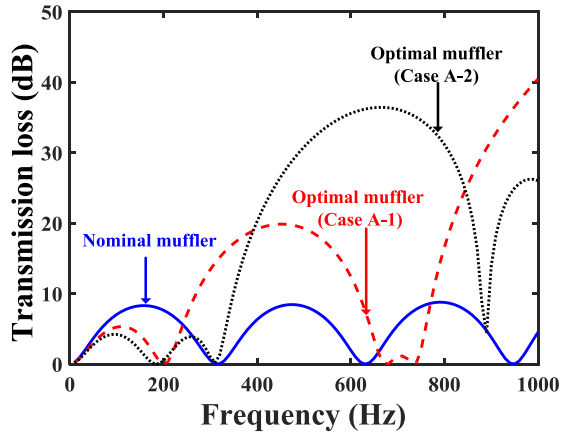

(a)

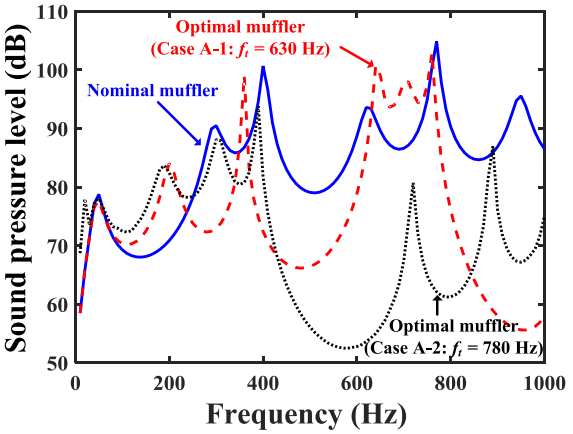

(b)

Fig. 8. Noise attenuation performance of optimal mufflers obtained by solving TL maximization problem: (a) comparison of TL curves and (b) comparison of measured SPL curves at target position when optimal mufflers are mounted on a duct. (Reference standard pressure: 20×10^{-6} Pa).

outlet. For $f_t = 780$ Hz with $V_r = 0.0662$, it seemed that Cases A-2 and B-2 had similar partition layouts. However, whereas only Case A-2 had horizontal partitions at the ends of all vertical partitions, Case B-2 had horizontal partitions with wide ends around the outlet and vertical partitions without horizontal partitions. Fig. 9(c) shows the optimization histories of the IL value at the target frequency with several intermediate and optimal topologies during the optimization process for both cases.

The IL curves of the optimal and nominal mufflers are compared in Fig. 10(a). The IL value at the target frequency in the optimal mufflers was sufficiently increased: $\Delta \mathrm{IL}_{f_t=630\ \mathrm{Hz}} = 30.40$ dB in Case B-1, and $\Delta \mathrm{IL}_{f_t=780\ \mathrm{Hz}} = 97.52$ dB in Case B-2. Fig. 10(b) compares the SPL curves at the target position P_{IV} when the optimal mufflers in Fig. 9(a) and (b) were individually mounted on a duct, as shown in Fig. 5(b). The SPL value at each target frequency in both cases (Cases B-1 and B-2) was sufficiently decreased. Fig. 10(c) and (d) shows the SPL distributions of the optimal muffler obtained in Case B-2 at 780 Hz and 870 Hz. While the low SPL value around the outlet end in Fig. 10(c) leads to a high IL value at 780 Hz, the low IL value at 870 Hz results from a high SPL value around the outlet in Fig. 10(d).

To physically interpret the partition layout of the optimal muffler, the optimal topology in Fig. 9(b) was modified by partially removing some partitions. Fig. 11 compares the SPLs of the modified optimal mufflers at the target frequency. Three partition groups were selectively removed: the horizontal partitions around the outlet were removed in Fig. 11(a), the right vertical partitions were removed in Fig. 11(b), the left vertical partitions were removed in Fig. 11(c), and all vertical partitions were removed in Fig. 11(d). The IL curves of the modified optimal mufflers are compared with that of the optimal topology in Fig. 11(e). It was found that the horizontal partitions and right vertical partitions contributed greatly to a low SPL value rather than the left vertical partitions.

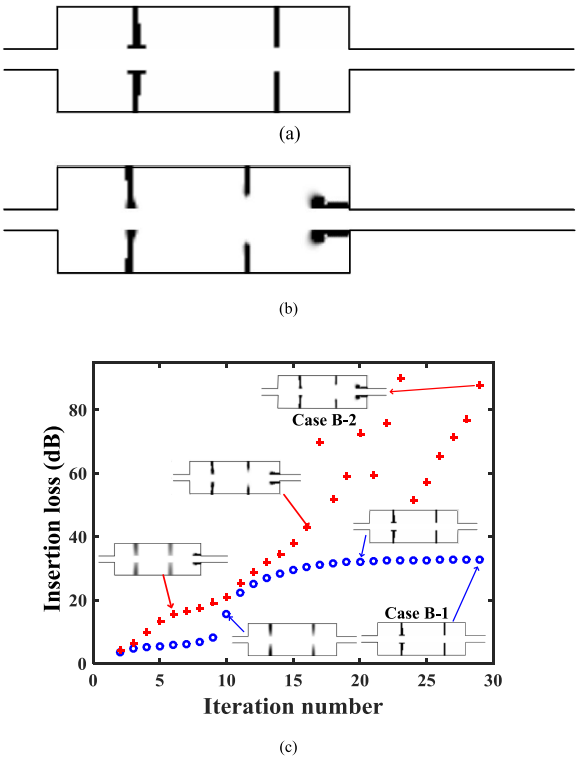

Fig. 9. Design results of IL maximization problem: (a) optimal topology in Case B-1, (b) optimal topology in Case B-2, and (c) optimization history.

To investigate the effects of the outlet length on an optimal design, the IL maximization problem was solved again at $f_t = 610$ Hz with $V_r = 0.0445$ for 41 cases: d_2 increased from 0.10 m to 0.50 m in increments of 0.01 m. The optimal topologies of all cases were horizontally symmetric, and the IL value of the optimal muffler at the target frequency was dramatically increased. Fig. 12 compares the optimal topologies of the representative eight cases, and their IL values are compared with those of the nominal muffler in Table 3: $d_2 = 0.10$ m for Case C-1, $d_2 = 0.11$ m for Case C-2, $d_2 = 0.18$ m for Case C-9, $d_2 = 0.19$ m for Case C-10, $d_2 = 0.23$ m for Case C-14, $d_2 = 0.24$ m for Case C-15, $d_2 = 0.46$ m for Case C-37, and $d_2 = 0.47$ m for Case C-38. Fig. 12(a) and (b) show that the optimal topology changed slightly for $\Delta d_2 = 0.01$ m in the majority of cases. However, an abrupt change in the number of vertical partitions was observed as shown in Fig. 12(c) and (d): a pair of vertical partitions were changed to two pairs of vertical partitions. By contrast, the number of vertical partitions decreased as shown in Fig. 12(e) and (f) when d_2 changed from 0.23 m to 0.24 m. It increased again as shown in Fig. 12(g) and (h) when d_2 changed from 0.46 m to 0.47 m.

In summary, the optimal topology changed almost continuously with the outlet length in its limit range, and the number of vertical partitions almost periodically changed as the outlet length increased. From these results, it was concluded that the optimal topology obtained by solving the IL maximization problem was strongly affected by the outlet length as well as the target frequency even for the same value of V_r. Therefore, in a topology-optimization-based muffler design problem using the IL as a method for evaluating the noise attenuation performance, the outlet length of a muffler unit for an acoustical analysis should be equal to the tailpipe length of a muffler mounted on a duct.

4. Optimal design and experimental validation

Considering the numerical analysis and design results in Section 3, we reached the conclusion that the use of the IL can decrease the discrepancy between the noise attenuation performance of an optimal muffler unit and an optimal muffler mounted on a duct. In addition, the accuracy of the IL calculated through a simulation depends on the accuracy of the radiation impedance at the outlet end. This motivated the authors to use the measured radiation impedances at the duct end, instead of the approximate equation in Eq. (16a), in the muffler design problem. In this section, another acoustical topology optimization problem is formulated for the optimal muffler design using the IL calculated based on the measured radiation impedance as a method for evaluating the noise attenuation performance. The noise attenuation performance of an optimally designed muffler is experimentally supported.

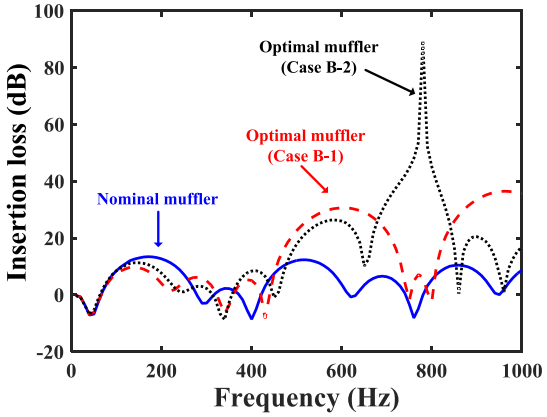

(a)

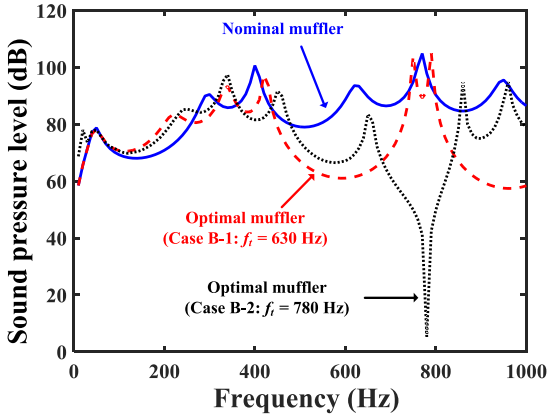

(b)

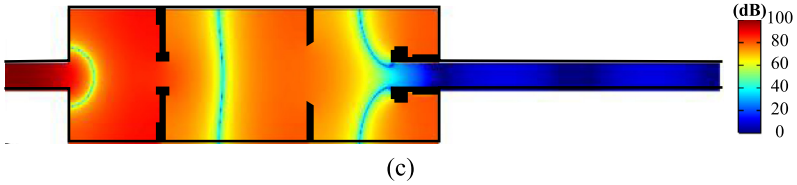

(c)

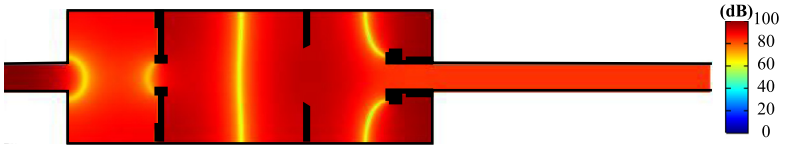

(d)

Fig. 10. Noise attenuation performance of optimal mufflers obtained by solving IL maximization problem: (a) comparison of IL curves, (b) comparison of measured SPL curves at target position when optimal mufflers are mounted on a duct (reference standard pressure: 20×10^{-6} Pa), (c) SPL distribution of optimal topology of Case B-2 at 780 Hz (reference standard pressure: 20×10^{-6} Pa), and (d) SPL distribution of optimal topology of Case B-2 at 870 Hz (reference standard pressure: 20×10^{-6} Pa).

4.1. Measured radiation impedance

An experimental setup using an impedance tube, as shown in Fig. 13(a), was used to measure the radiation impedance at the end of the square duct. The length h_d of one side of the square duct was 0.04 m, the thickness t_d of the duct wall was 0.10 m, the distance s_d between the two microphones was 0.025 m, and the distance between Microphone 2 and the end of the duct was 0.165 m. The cutoff frequency of this duct was 4287.5 Hz. A speaker (DU-75, InterM) was mounted at the left end of the duct for incident acoustic wave generation, and two microphones (Type 46BE, GRAS) were mounted around the right

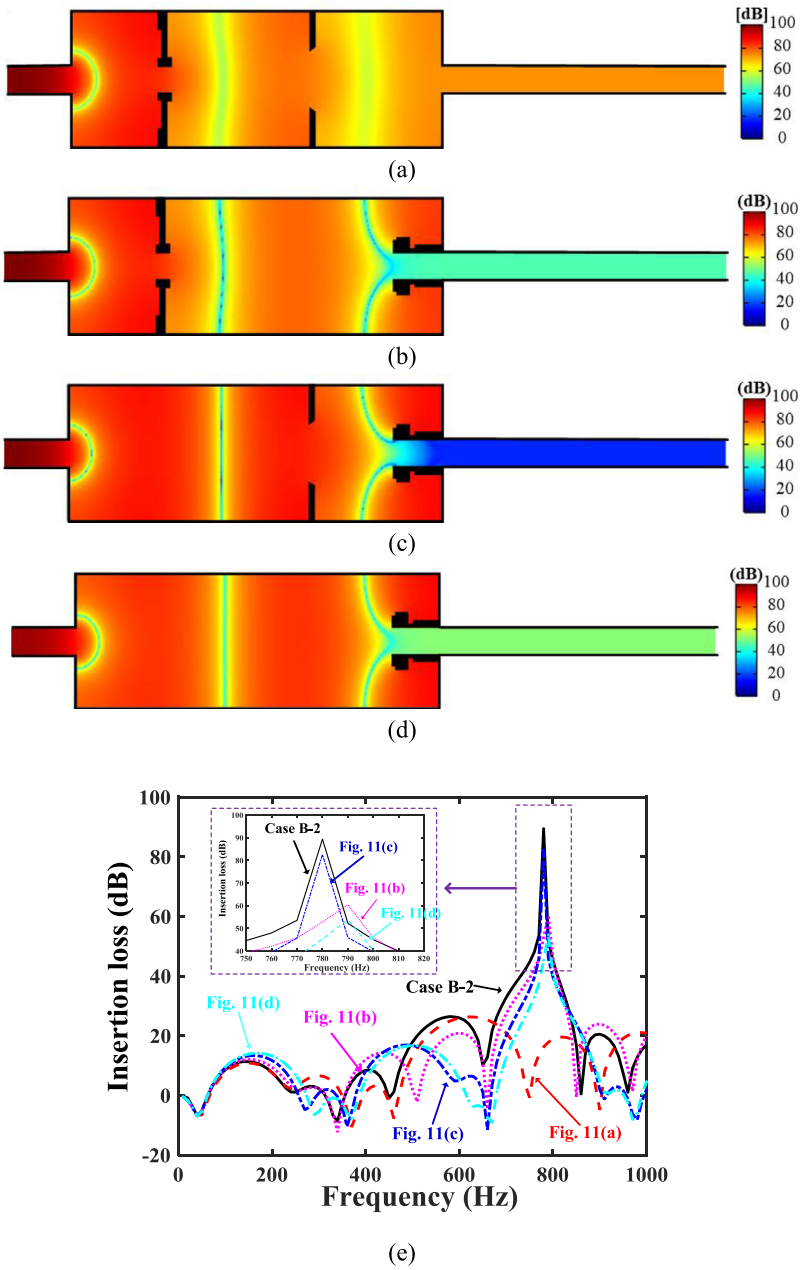

Fig. 11. Comparison of modified optimal mufflers: (a) SPL distribution in 1st modified optimal muffler (reference standard pressure: 20×10^{-6} Pa), (b) SPL distribution in 2nd modified optimal muffler (reference standard pressure: 20×10^{-6} Pa), (c) SPL distribution in 3rd modified optimal muffler (reference standard pressure: 20×10^{-6} Pa), (d) SPL distribution in 4th modified optimal muffler (reference standard pressure: 20×10^{-6} Pa), and (e) IL curves of modified optimal mufflers.

end to measure the acoustic pressures at two points. The microphones were denoted as "Microphone 1" and "Microphone 2." The absorption-testing module of the LMS Test Lab hardware/software package was used to generate a pseudorandom signal, which was fed to a speaker through an amplifier, and to acquire the microphone signals. The frequency resolution was set to 1 Hz. Fig. 13(b) and (c) compare the real and imaginary parts of the measured and calculated dimensionless radiation impedance curves, which agreed well with each other in a low-frequency range except around 0 Hz. However, the difference between the two curves increased with the frequency. The difference of the two curves around 0 Hz was owing to noise caused by the poor excitation performance of the used speaker. Some noise around 0 Hz existed even after a 100-time averaging process. It was concluded that because the appropriate equation in Eq. (16) was valid only in an extremely low-frequency range, the measured radiation impedance should be used to calculate the IL at the target frequency for this muffler design problem.

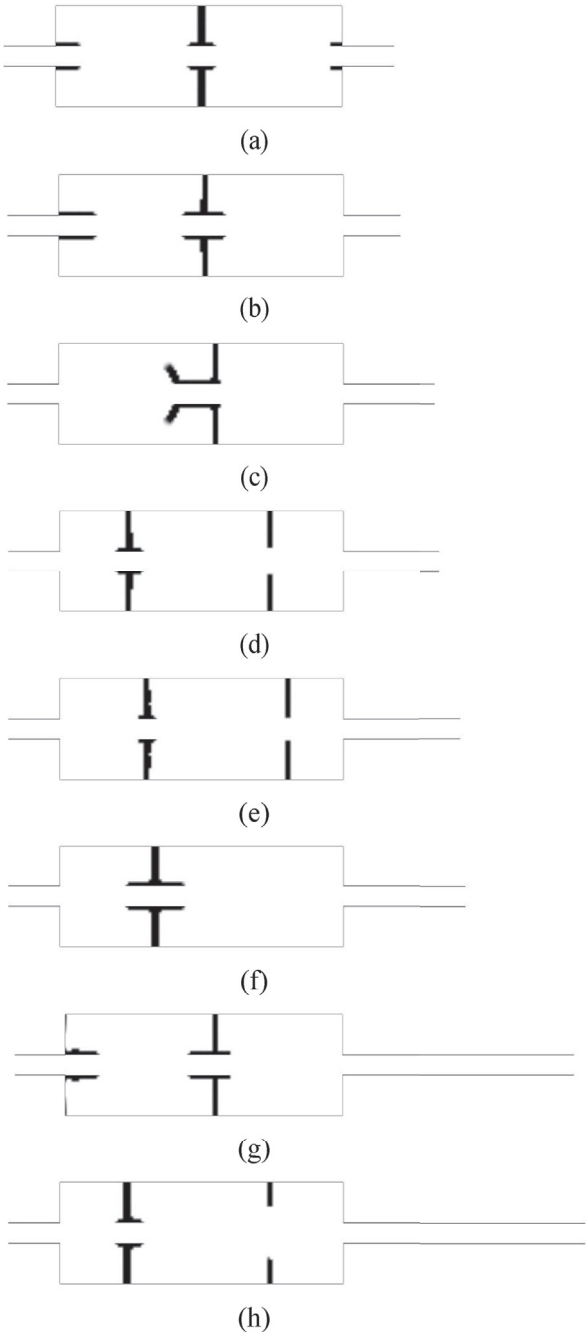

Fig. 12. Optimal topologies depending on outlet length at 610 Hz: (a) $d_2 = 0.10$ m in Case C-1, (b) $d_2 = 0.11$ m in Case C-2, (c) $d_2 = 0.18$ m in Case C-9, (d) $d_2 = 0.19$ m in Case C-10, (e) $d_2 = 0.23$ m in Case C-14, (f) $d_2 = 0.24$ m in Case C-15, (g) $d_2 = 0.46$ m in Case C-37, and (h) $d_2 = 0.47$ m in Case C-38.

4.2. Optimal muffler

The partition volume minimization problem [28] for an optimal muffler design was recalled and modified, and the TL was replaced with the IL. The volume of the rigid partitions was selected as an objective function in Eq. (25a), and the IL values at several frequencies in the target frequency range were constrained as in Eq. (25b).

$$\min \text{obj}, \text{obj} = \int \chi_r dV, \tag{25a}$$

Table 3
Effects of outlet pipe length on optimization design results for $f_t = 610$ Hz and $V_r = 0.0445$ for eight cases.

Case	d_2 (m)	$IL_{nominal}$ (dB)	$IL_{optimal}$ (dB)	ΔIL(dB)
C-1	0.10	10.48	13.70	3.23
C-2	0.11	9.77	15.45	5.68
C-9	0.18	−5.75	85.26	91.01
C-10	0.19	−10.81	26.99	37.80
C-14	0.23	4.82	19.87	15.05
C-15	0.24	6.53	18.06	11.53
C-37	0.46	−4.82	6.60	11.41
C-38	0.47	−10.59	24.18	34.78

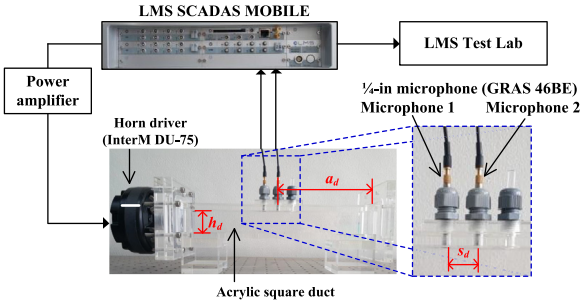

(a)

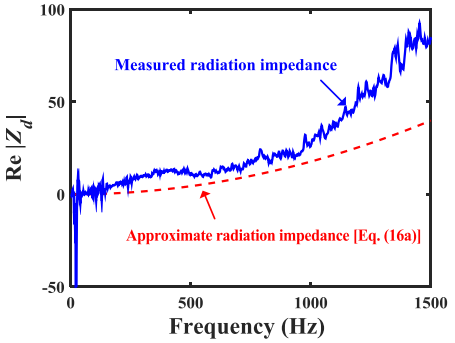

(b)

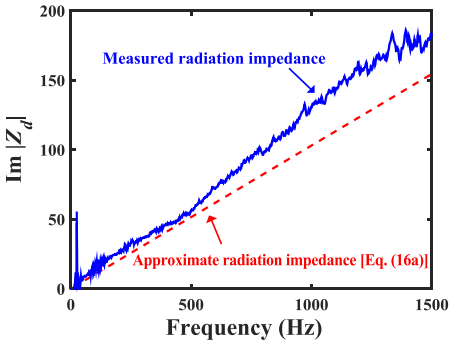

(c)

Fig. 13. Radiation impedance measurement: (a) experimental setup, (b) comparison of real parts of measured radiation impedance and approximate radiation impedance in Eq. (16a), and (c) comparison of imaginary parts of measured radiation impedance and approximate radiation impedance in Eq. (16a). All radiation impedance values were converted to dimensionless values by dividing Z_d by $(Z_0 \cdot S)$, where S is cross-sectional area of a duct.

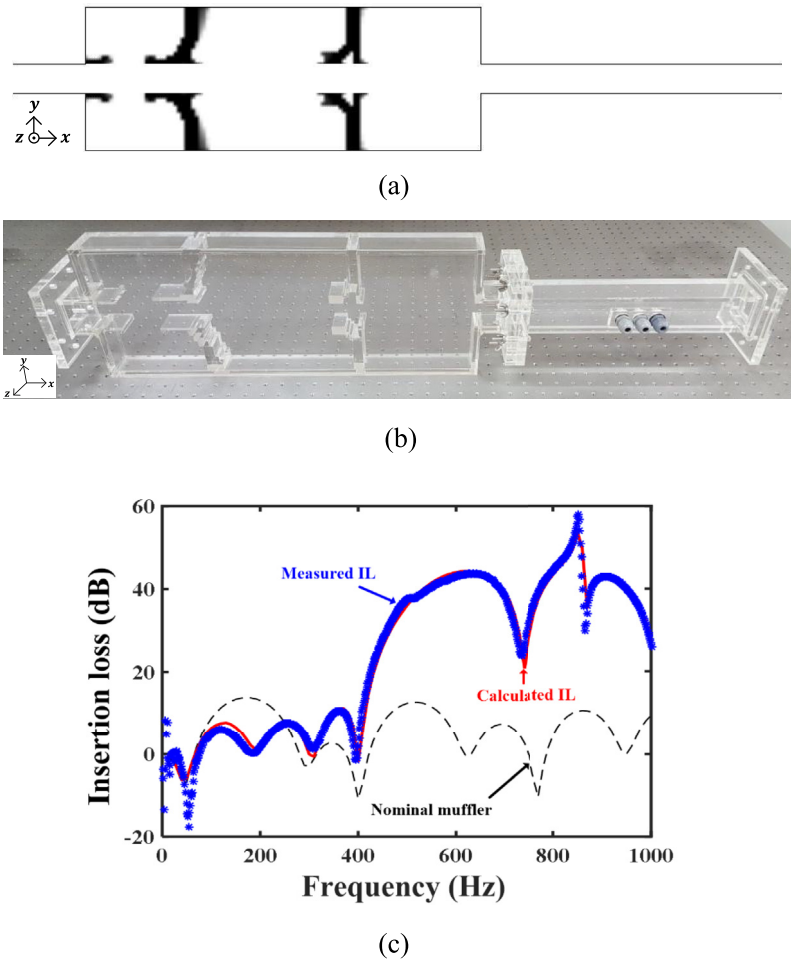

Fig. 14. Optimal design and experimental validation: (a) optimal topology obtained by solving partition volume minimization problem, (b) acrylic muffler corresponding to optimal topology shown in (a), and (c) comparison of simulated and measured IL curves.

$$\mathrm{IL}_{\mathrm{low}} \le \mathrm{IL}_{f=f_i}, f_i (i = 1, 2, \ldots, N), f_{\mathrm{low}} \le f_i \le f_{\mathrm{upp}}, \Delta f = f_{i+1} - f_i, \tag{25b}$$

where f_{low} and f_{upp} represent the lower- and upper-limit frequencies of the target frequency range, respectively. The same interpolation functions in Eqs. (23a) and (23b) were used.

The formulated topology optimization problem was solved for $f_{\mathrm{low}} = 700$ Hz, $f_{\mathrm{upp}} = 900$ Hz, $\Delta f = 20$ Hz, and $\mathrm{IL}_{\mathrm{low}} = 25$ dB by following the iterative calculation algorithm in Fig. 6(b). The final topology in Fig. 14(a) had some design variables (gray colors) that were neither 0 nor 1 at the left-hand side vertical partitions and was postprocessed for a validation experiment: all design variables were forcibly rounded off to "0" or "1." The two-dimensional muffler in Fig. 14(a) was extruded along the z-direction to make a three-dimensional acrylic muffler, as shown in Fig. 14(b), with a thickness of 0.04 m. By using the experimental setup in Ref. [28], the IL curve of the optimal muffler in Fig. 14(b) was obtained using the LMS Test Lab hardware/software package. Fig. 14(c) compares the measured and calculated IL curves of the optimized muffler shown in Fig. 14(b). The two IL curves agreed well with each other in the entire frequency range.

5. Conclusions

In this work, three methods (TL, IL, and LD) to evaluate the noise attenuation performance of a muffler were theoretically and computationally investigated for decreasing the discrepancy between the noise attenuation performances of an optimal muffler unit and an optimal muffler mounted on a duct. Mathematical expressions for the TL, IL, and LD described the effects of the locations of the measurement points, tailpipe length, and impedance at the duct on the noise attenuation performance calculated using the three evaluation methods. Because the LD was strongly affected by the locations of the measurement points as well as the tailpipe length and impedance at the duct end, the noise attenuation performance of a muffler unit could

not be objectively evaluated. To compare the TL and IL, two acoustical topology optimization problems for TL and IL maximization were formulated for a muffler unit design and were solved for the same design conditions. Because the TL formula was defined for anechoic termination condition, it could not accurately predict the in-duct noise reduction when an optimally designed muffler was mounted on a duct. By contrast, a muffler designed optimally using the IL as an evaluation method could actually reduce the in-duct noise when mounted on a duct only if the tailpipe length and the impedance at the duct were accurately used in the formulated muffler design problem.

In short, if the noise attenuation performance of a muffler in the frequency range of interest is obviously affected by the acoustic characteristics of its expansion chamber only, TL might be used as an evaluation index in a muffler design problem. However, IL should be used if the noise attenuation performance of a muffler in the frequency range of interest is affected by the tailpipe length as well as the acoustic characteristics of the expansion chamber.

To confirm the accuracy of optimal mufflers designed using the IL, a partition volume minimization problem with a moderate IL value in the target frequency range was formulated, and the noise attenuation performance of a muffler designed optimally for broadband noise reduction was validated experimentally. These research results will contribute to reducing the discrepancy between the noise attenuation performances of a muffler unit and a muffler mounted on a duct. If they are combined with the precise calculated flow analysis results, they can be applied to duct noise reduction problems in the field of HVAC.

Acknowledgements

This research was supported by the Basic Science Research Program through the National Research Foundation of Korea (NRF) funded by the Ministry of Education (No. 2016R1D1A1B03932357).

Appendix A. Derivation of sound intensity for calculation of IL

The sound intensity ($I_{w/o}$) in a duct without a muffler, as shown in Fig. 1(a), is expressed as a function of the acoustic pressure and particle velocity in a complex value form, as indicated in Eq. (A.1). Using Eqs. (1) and (2a), Eq. (A.1) is converted into Eq. (A.2). Considering that $A_0A_0^*$ and $R_{w/o}R_{w/o}^*$ are real values, Eq. (A.2) is converted into Eq. (A.3). If the second term in Eq. (A.3) is arranged using the Euler formula [43], then Eq. (A.3) is converted into Eq. (A.4). Considering that $R_{w/o} - R_{w/o}^*$ and $R_{w/o} + R_{w/o}^*$ are a purely imaginary value and a real value, respectively, Eq. (A.4) is converted into Eq. (A.5).

$$I_{w/o} = \frac{1}{2}\mathrm{Re}\{p_0(x)u_0^*(x)\}, \tag{A.1}$$

$$I_{w/o} = \frac{1}{2\rho c}\mathrm{Re}\left\{A_0A_0^*\left(1 + R_{w/o}e^{-j2k(l+d-x)} - R_{w/o}^*e^{j2k(l+d-x)} - R_{w/o}R_{w/o}^*\right)\right\}, \tag{A.2}$$

$$I_{w/o} = \frac{1}{2\rho c}\left[\left(A_0A_0^*\left(1 - R_{w/o}R_{w/o}^*\right)\right) + \mathrm{Re}\left\{R_{w/o}e^{-j2k(l+d-x)} - R_{w/o}^*e^{j2k(l+d-x)}\right\}\right], \tag{A.3}$$

$$I_{w/o} = \frac{1}{2\rho c}\begin{bmatrix}\left(A_0A_0^*\left(1 - R_{w/o}R_{w/o}^*\right)\right)\\ +\mathrm{Re}\left\{\left(R_{w/o} - R_{w/o}^*\right)\cos(2k(l+d-x))\right\}\\ -\mathrm{Re}\left\{j\left(R_{w/o} + R_{w/o}^*\right)\sin(2k(l+d-x))\right\}\end{bmatrix}, \tag{A.4}$$

$$I_{w/o} = \frac{1}{2\rho c}\left(A_0A_0^*\left(1 - R_{w/o}R_{w/o}^*\right)\right). \tag{A.5}$$

The sound intensity (I_w) in an outlet of a muffler, as shown in Fig. 1(b), is expressed as a function of the acoustic pressure and particle velocity in a complex value form, as in Eq. (A.6). In the same way as in a duct without a muffler, Eq. (A.6) is converted into Eq. (A.7).

$$I_w = \frac{1}{2}\mathrm{Re}\{p_3(x)u_3^*(x)\}, \tag{A.6}$$

$$I_w = \frac{1}{2\rho c}\left(A_3A_3^*(1 - R_wR_w^*)\right). \tag{A.7}$$

Appendix B. Four-microphone method

In Fig. 5(c) and (d), acoustic pressures (p_a, p_b, p_c, and p_d) at two points in the inlet and at two points in the outlet using Eqs. (3a) and (3c) are expressed through Eqs. (B.1)–(B.4) for $l = l_1$ and $d = d_1$ or $d = d_2$. The amplitude (A_1) of the forward traveling wave in an inlet is derived from Eqs. (B.1) and (B.2), as expressed in Eq. (B.5). The amplitude (A_3) of the forward traveling wave in an outlet is derived as expressed in Eq. (B.6) in the same way as for A_1.

$$p_a = p_1(-m_1 - s_1) = A_1 e^{-jk(-m_1-s_1)} + B_1 e^{jk(-m_1-s_1)}, \tag{B.1}$$

$$p_b = p_1(-m_1) = A_1 e^{-jk(-m_1)} + B_1 e^{jk(-m_1)}, \tag{B.2}$$

$$p_c = p_3(l_1 + m_2) = A_3 e^{-jk(m_2-d)} + B_3 e^{jk(m_2-d)}, \tag{B.3}$$

$$p_d = p_3(l_1 + m_2 + s_2) = A_3 e^{-jk(m_2+s_2-d)} + B_3 e^{jk(m_2+s_2-d)}, \tag{B.4}$$

$$A_1 = \frac{\left(p_a e^{jks_1} - p_b\right) e^{-jk(m_1+s_1)}}{e^{jks_1} - e^{-jks_1}}, \tag{B.5}$$

$$A_3 = \frac{\left(p_c e^{jks_2} - p_d\right) e^{jk(m_2-d)}}{e^{jks_2} - e^{-jks_2}}. \tag{B.6}$$

As expressed in Eqs. (10) and (14), Γ is expressed as a function of A_1/A_3. When substituting Eqs. (B.5) and (B.6) for A_1 and A_3 in Eqs. (10) and (14), respectively, the TL and IL are calculated using Eq. (B.7) with four acoustic pressures (p_a, p_b, p_c, and p_d).

$$\Gamma = 10\log_{10}\left|\frac{\left(p_a e^{jks_1} - p_b\right)}{\left(p_c e^{jks_2} - p_d\right)}\frac{e^{jks_2} - e^{-jks_2}}{e^{jks_1} - e^{-jks_1}}\right|^2. \tag{B.7}$$

References

[1] M.L. Munjal, Acoustics of Ducts and Mufflers, second ed., John Wiley & Sons, New York, 2014.
[2] J.D. Irwin, E.R. Graf, Industrial Noise and Vibration Control, Prentice-Hall, New Jersey, 1979.
[3] M.G. Prasad, M.J. Crocker, Studies of acoustical performance of a multi-cylinder engine exhaust muffler system, J. Sound Vib. 90 (1983) 491–508.
[4] S. Bilawchuk, K.R. Fyfe, Comparison and implementation of the various numerical methods used for calculating transmission loss in silencer systems, Appl. Acoust. 64 (2003) 903–916.
[5] M. Åbom, Derivation of four-pole parameters including higher order mode effects for expansion chamber mufflers with extended inlet and outlet, J. Sound Vib. 137 (1990) 403–418.
[6] A. Selamet, P.M. Radavich, The effect of length on the acoustic attenuation performance of concentric expansion chambers: an analytical, computational and experimental investigation, J. Sound Vib. 201 (1997) 407–426.
[7] R. Kirby, Simplified techniques for predicting the transmission loss of a circular dissipative silencer, J. Sound Vib. 243 (2001) 403–426.
[8] X. Yu, L. Cheng, Duct noise attenuation using reactive silencer with various internal configurations, J. Sound Vib. 335 (2015) 229–244.
[9] Z. Tao, A.F. Seybert, A Review of Current Techniques for Measuring Muffler Transmission Loss, SAE Technical Paper 2003-01-1653, 2003.
[10] M.G. Prasad, M.J. Crocker, Insertion loss studies on models of automotive exhaust systems, J. Acoust. Soc. Am. 70 (1981) 1339–1344.
[11] A. Craggs, A finite element method for damped acoustic systems: an application to evaluate the performance of reactive mufflers, J. Sound Vib. 48 (1976) 377–392.
[12] R. Ramakrishnan, R. Stevens, Improving the accuracy of duct silencer insertion loss predictions, J. Sound Vib. 194 (1976) 423–427.
[13] J. Krüger, P. Leistner, Noise reduction with actively absorbing silencers, Appl. Acoust. 51 (1997) 113–120.
[14] D.W. Herrin, S. Ramalingam, Z. Cui, J. Liu, Predicting insertion loss of large duct systems above the plane wave cutoff frequency, Appl. Acoust. 73 (2012) 37–42.
[15] K.N. Rao, M.L. Munjal, Noise reduction with perforated three-duct muffler components, Sādhanā 9 (1986) 255–269.
[16] H. Levine, J. Schwinger, On the radiation of sound from an unflanged circular pipe, Phys. Rev. 73 (1948) 383–406.
[17] A.N. Norris, I.C. Sheng, Acoustic Radiation from a circular pipe with an infinite flange, J. Sound Vib. 135 (1989) 85–93.
[18] F. Silva, P. Guillemain, J. Kergomard, B. Mallaroni, A.N. Norris, Approximation formulae for the acoustic radiation impedance of a cylindrical pipe, J. Sound Vib. 322 (2009) 255–263.
[19] J.D. Polack, X. Meynial, J. Kergomard, C. Cosnard, M. Bruneau, Reflection function of a plane sound wave in a cylindrical tube, Rev. Phys. Appl. 22 (1987) 331–337.
[20] J.P. Dalmont, Acoustic impedance measurement, part I: a review, J. Sound Vib. 243 (2001) 427–439.
[21] J.P. Dalmont, C.J. Nederveen, N. Joly, Radiation impedance of tubes with different flanges: numerical and experimental investigations, J. Sound Vib. 244 (2001) 505–534.
[22] L. Huang, Parametric study of a drum-like silencer, J. Sound Vib. 269 (2004) 467–488.
[23] R. Barbieri, N. Barbieri, Finite element acoustic simulation based shape optimization of a muffler, Appl. Acoust. 67 (2006) 346–357.
[24] R. Barbieri, N. Barbieri, The technique of active/inactive finite elements for the analysis and optimization of acoustical chambers, Appl. Acoust. 73 (2012) 184–189.
[25] K. Fonseca De Lima, A. Lenzi, R. Barbieri, The study of reactive silencers by shape and parametric optimization techniques, Appl. Acoust. 72 (2011) 142–150.
[26] J.W. Lee, Y.Y. Kim, Topology optimization of muffler internal partitions for improving acoustical attenuation performance, Int. J. Numer. Methods Eng. 80 (2009) 455–477.

[27] J.W. Lee, G.W. Jang, Topology design of reactive mufflers for enhancing their acoustic attenuation performance and flow characteristics simultaneously, Int. J. Numer. Methods Eng. 91 (2012) 552–570.
[28] J.W. Lee, Optimal topology of reactive muffler achieving target transmission loss values: design and experiment, Appl. Acoust. 88 (2015) 104–113.
[29] K.S. Oh, J.W. Lee, Two-step design process for optimal suction muffler in reciprocating compressor, J. Mech. Sci. Technol. 29 (2015) 269–278.
[30] G.W. Jang, J.W. Lee, Topology optimization of internal partitions in a flow-reversing chamber muffler for noise reduction, Struct. Multidiscip. Optim. 55 (2017) 2181–2196.
[31] K.S. Oh, J.W. Lee, Topology optimization for enhancing the acoustical and thermal characteristics of acoustic devices simultaneously, J. Sound Vib. 401 (2017) 54–75.
[32] X. Yu, Y. Tong, J. Pan, L. Cheng, Sub-chamber optimization for silencer design, J. Sound Vib. 351 (2015) 57–67.
[33] E.L. Yedeg, E. Wadbro, M. Berggren, Interior layout topology optimization of a reactive muffler, Struct. Multidiscip. Optim. 53 (2016) 645–656.
[34] B.S. Sridhara, M.J. Croker, Review of theoretical and experimental aspects of acoustical modeling of engine exhaust systems, J. Acoust. Soc. Am. 95 (1994) 2363–2370.
[35] R.C. Chanaud, Effects of geometry on the resonance frequency of Helmholtz resonators, J. Sound Vib. 178 (3) (1994) 337–348.
[36] R.C. Chanaud, Effects of geometry on the resonance frequency of Helmholtz resonators, part II, J. Sound Vib. 204 (5) (1997) 829–834.
[37] M.L. Pollack, The acoustic inertial end correction, J. Sound Vib. 67 (4) (1979) 558–661.
[38] H. Bukac, Acoustic filters: part II: the four-microphone method of experimental verification of acoustic characteristics of mufflers, in: Int. Compress. Eng. Conf., 2006. C083-1-8.
[39] G.H. Yoon, Acoustic topology optimization of fibrous material with Delany-Bazley empirical material formulation, J. Sound Vib. 322 (2013) 1172–1187.
[40] J.W. Lee, Y.Y. Kim, Rigid body modeling issue in acoustical topology optimization, Comput. Methods Appl. Math. 198 (2009) 1017–1030.
[41] K. Svanberg, The method of moving asymptotes—a new method for structural optimization, Int. J. Numer. Methods Eng. 24 (1987) 359–373.
[42] M.B. Dühring, J.S. Jensen, O. Sigmund, Acoustic design by topology optimization, J. Sound Vib. 317 (2008) 557–575.
[43] E. Kreyszig, Advanced Engineering Mathematics, John Wiley & Sons, New York, 2006.